Wang et al. Nanoscale Research Letters (2017) 12:619
DOI 10.1186/s11671-017-2393-1

Nanoscale Research Letters

NANO EXPRESS Open Access

Hybrid UV-Ozone-Treated rGO-PEDOT:PSS as an Efficient Hole Transport Material in Inverted Planar Perovskite Solar Cells

Shuying Wang[1,2], Xiaona Huang[1,3], Haoxuan Sun[1] and Chunyang Wu[1*]

Abstract

Inverted planar perovskite solar cells (PSCs), which are regarded as promising devices for new generation of photovoltaic systems, show many advantages, such as low-temperature film formation, low-cost fabrication, and smaller hysteresis compared with those of traditional n-i-p PSCs. As an important carrier transport layer in PSCs, the hole transport layer (HTL) considerably affects the device performance. Therefore, HTL modification becomes one of the most critical issues in improving the performance of PSCs. In this paper, we report an effective and environmentally friendly UV-ozone treatment method to enhance the hydrophilia of reduced graphene oxide (rGO) with its excellent electrical performance. The treated rGO was applied to doped poly(3,4-ethylenedioxythiophene) poly(styrene-sulfonate) (PEDOT:PSS) as HTL material of PSCs. Consequently, the performance of rGO/PEDOT:PSS-doped PSCs was improved significantly, with power conversion efficiency (PCE) of 10.7%, *Jsc* of 16.75 mA/cm^2, *Voc* of 0.87 V, and FF of 75%. The PCE of this doped PSCs was 27% higher than that of the PSCs with pristine PEDOT:PSS as HTL. This performance was attributed to the excellent surface morphology and optimized hole mobility of the solution-processable rGO-modified PEDOT:PSS.

Keywords: Inverted planar perovskite solar cells, Reduced graphene oxide (rGO), UV-ozone treatment, PEDOT:PSS

Background

As one of the world's top 10 scientific and technological breakthroughs in 2013, hybrid organic–inorganic perovskite material is regarded as one of the most promising materials for developing high-efficient photovoltaic devices because of its excellent photoelectric property [1–3]. In the past 7 years, the power conversion efficiency (PCE) of perovskite solar cells (PSCs) has increased remarkably from 3.8 to 22.1%, which outperforms those of conventional polycrystalline silicon solar cells [4]. Unfortunately, the traditional manufacture of n-i-p-type PSCs involving high-temperature annealing procedure is unavailable to flexible substrates, thereby limiting its commercial prospects. The novel solar cell device, which was first fabricated by Guo et al. in 2013 and delivered a PCE 3.9% [5], consists of poly(3,4-ethylenedioxythiophene) poly(styrene-sulfonate) (PEDOT:PSS) as the hole transport layer (HTL) and [6,6]-phenyl C61-butyric acid methyl ester as electron transport layer (ETL). Specifically, the p-type hole transport material (HTM) is deposited prior to the perovskite light absorption film. Subsequently, the n-type ETL is deposited onto the perovskite film. This p-i-n architecture is an inverted structure, which shows many excellent properties, such as easy fabrication, cost-effectiveness, small hysteresis, and high fill factor, compared with those of traditional n-i-p devices [6–8]. To date, the inverted planar PCSs have attracted considerable interest [9, 10]. Researchers used a variety of methods, including structure optimization [11–13], development of improved HTL [13] and ETL [14, 15], crystalline and morphology control of perovskites [16, 17], and interfacial engineering [18–20], to improve the efficiency of inverted PSCs. Unfortunately, the efficiency of inverted planar solar cells is still lower than that of traditional structure [21].

Graphene is a kind of 2D carbon nanomaterial that is composed of sp^2-hybridized carbon atoms in a hexagonal

* Correspondence: wucyzju@163.com
[1]State Key Laboratory of Electronic Thin Films and Integrated Devices, University of Electronic Science and Technology of China, Chengdu 610054, China
Full list of author information is available at the end of the article

structure [22]. This material possesses excellent advantages in electrical conductivity, optical transparency, and environment stability [23, 24]. HTL modification is one of the most important issues for improving the performance of inverted planar PSCs. For example, Yeo et al. applied reduced graphene oxide (rGO) nanosheets as HTLs, and the rGO-basic solar cell depicted a superior device efficiency (10.8%) to PEDOT:PSS- and GO-based solar cells [25]. Jokar et al. discussed the charge-extraction behavior of GO and rGO as p-contact layers for PSCs, demonstrating that the rGO synthesized via GO reduction with reducing agents obtains high-performance inverted planar heterojunction PSCs [26]. Moreover, graphene materials can serve as remarkable dopants to modify charge transport layer due to their long hot-electron lifetimes and ultrafast hot-electron extraction properties [27]. However, commercial graphene materials, such as rGO, aggregate when dispersed in water because of the absence of hydrophilic functional groups. GO exhibits low conductivity due to the damaged conjugated structure. Thus, a solution-processable graphene possessing both excellent electrical properties, such as rGO, and good dispersion characteristics, such as GO, should be well manufactured for HTL modification.

In this paper, we present a simple and environmentally friendly UV-ozone treatment method to obtain water-dispersed graphene with high charge mobility. Furthermore, we doped PEDOT:PSS using the obtained graphene to form an improved HTM in inverted PSCs. The incorporation of treated graphene into PEDOT:PSS increased the short-circuit current density and PCE of the PSCs. A remarkably enhanced *V*oc of 0.87 V with a relatively high J_{SC} of 16.75 mA/cm^2 was obtained. The corresponding PCE with an average value of 10.75% was achieved with high reproducibility. The typical PCE of PSCs with rGO/PEDOT:PSS was improved by 27% compared with that of PSCs with pristine PEDOT:PSS as HTL.

Methods/Experimental

Chemicals

PEDOT:PSS (CleviosTM PVP. Al 4083) and CH_3NH_3I (MAI) were purchased from Heraeus Materials Technology Shanghai Ltd. and Deysol Ltd., respectively. PbI_2 (99%), anhydrous *N*,*N*-dimethylformamide (DMF, 99.8%), and anhydrous chlorobenzene (CB, 99.8%) were supplied by Sigma-Aldrich company. [6,6]-Phenyl-C_{61}-butyric acid methyl ester (PC61BM, > 99%) and 2,9-dimethyl-4,7-diphenyl-1,10-phenanthroline (BCP, > 99%) were obtained from Xi'an Polymer Light Technology Corp. rGO was synthesized by Y.F. Chen's Team [28].

Solution Preparation

Approximately 5 mg of rGO was placed in a quartz Petri dish and subsequently treated with UV-ozone cleaning procedure (operating power, 270 W) continuously for 2 h. Afterward, the obtained rGO was collected and added into deionized water to form a solution with the concentration of 1 mg/mL under ultrasonic bath treatment.

To obtain improved HTM for inverted PSCs, rGO solutions with different volume ratios (0.1, 0.2, and 0.3) were added into PEDOT:PSS solution at room temperature. The resultant rGO/PEDOT:PSS solutions were magnetically stirred overnight and filtered by polytetrafluoroethylene (PTFE) filters (0.45 μm).

The perovskite precursor solution was prepared by the following processes. MAI and PbI_2 powder were mixed in anhydrous DMF with a molar ratio of 1:1. Subsequently, the solution (40 wt%) was stirred overnight at 60 °C and filtered with 0.45-μm PTFE filters prior to device fabrication.

Device Fabrication

The structure of the inverted planar heterojunction PSCs was indium tin oxide (ITO)/PEDOT:PSS/$CH_3NH_3PbI_3$/$PC_{61}BM$/BCP/Ag. The ITO substrate (1.5 × 1.5 cm^2) was cleaned sequentially with acetone, isopropanol, and deionized water. The prepared UV-ozone-treaded rGO/PEDOT:PSS solution was spin coated to film at 4000 rpm for 40 s and thermally treated at 150 °C for 10 min in air. In this treatment, the perovskite active layer was deposited by one-step solution method through spin coating $CH_3NH_3PbI_3$ precursor solution (40 wt% in DMF) at 4000 rpm for 40 s. To improve the crystallization of the active layer, 70 μL of CB was dropped quickly onto $CH_3NH_3PbI_3$ wet film at approximately 6 s after the beginning of spinning, as reported in the literature [29]. The films were annealed at 110 °C for 30 min inside the glove box filled with nitrogen. Afterward, a solution of PC61BM in CB (20 mg/mL) was spin coated onto the perovskite film at 3000 rpm for 40 s. Subsequently, saturated BCP solution was spin coated in isopropyl alcohol at 2000 rpm for 30 s. Finally, a Ag layer (100 nm) was deposited by thermal evaporation.

Characterization

The component analysis of rGO was conducted by X-ray photoelectron spectroscopy (XPS) with an ESCALAB 250 electron spectrometer. The crystallization structures of $CH_3NH_3PbI_3$ layers were determined by X-ray diffraction (XRD Bede multifunctional high-resolution X-ray diffractometer, British). The film morphology was observed by atomic force microscopy (AFM, SPI3800, Japan). The current density–voltage (J–V) measurement was carried out by using Keithley model 2400 Source Meter under simulated AM 1.5 G solar illumination (100 mW/cm^2) generated by solar simulator (ABET Technologies, SUN 3000).

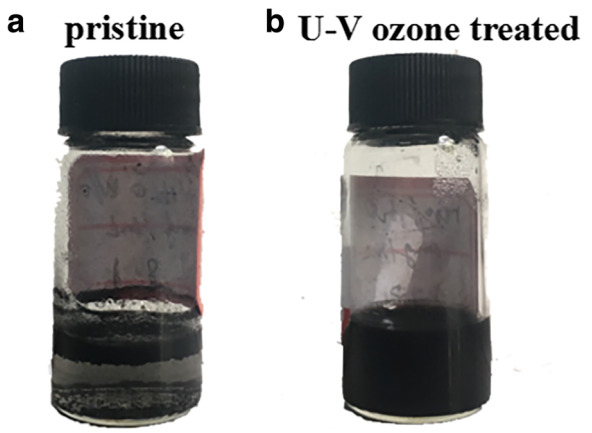

Fig. 1 Photographs of **a** untreated and **b** UV-ozone-treated rGO solution (1 mg/mL in H_2O)

Results and Discussion

The untreated and UV-ozone-treated rGOs dissolved in deionized water with the concentration of 1 mg/mL are shown in Fig. 1. The untreated rGO can be hardly dispersed in deionized water, and the treated one can be homogeneously dispersed in water, which is attributed to some –OH and –COOH groups in rGO. The UV-ozone-treated rGO solution still shows a deep black color compared with the brown 1 mg/mL commercial GO solution [22], thereby indicating the incomplete oxidation process of UV-ozone treatment.

XPS measurement was performed to verify whether parts of the oxygen-containing groups of rGO underwent hydrophilic treatment. As shown in Fig. 2a, the C1s spectra of untreated rGO clearly present a high degree of oxidation with four functional groups corresponding to C–C (non-oxygenated ring C, 284.7 eV), C–O (C in C–O bonds, 286.1 eV), C=O (carbonyl C, 287.2 eV), and C–(O)–OH (carboxyl groups, 288.8 eV) [30]. For rGO moderately treated with UV ozone, the intensities of peaks assigned to C–O and C–(O)–OH increase slightly. The intensity of peaks assigned to C–O and C–(O)–OH increases more evidently than that of C=O. Therefore, rGO treated with UV ozone can validly induce hydrophilic group.

XRD spectra were obtained to investigate the crystallization structure of $CH_3NH_3PbI_3$ layers. $CH_3NH_3PbI_3$ thin films were spin coated on pristine PEDOT:PSS and rGO/PEDOT:PSS HTLs and subsequently annealed at 100 °C for 30 min. As shown in Fig. 3, both perovskite films exhibit similar features and show three peaks at 14.14°, 28.08°, and 31.86°, which are associated with the (110), (220), and (310) planes of perovskite crystals, respectively. Nevertheless, perovskite coated on hybrid rGO/PEDOT:PSS layer displays sharper diffraction peaks than those coated on original PEDOT:PSS, which suggested the improved crystallinity of perovskite on modified PEDOT:PSS layer.

AFM was carried out to investigate the effect of rGO incorporation on PEDOT:PSS. Figure 4 shows the top-view AFM images of PEDOT:PSS and rGO/PEDOT:PSS thin films. These AFM top-view images of rGO/PEDOT:PSS thin films reveal no evident sign of rGO in the scanned area. This result is attributed to that the rGO is in the middle of PEDOT:PSS layer with a sandwich-like structure. In addition, the root-mean-square (RMS) roughness of pristine PEDOT:PSS layer is approximately 1.15 nm. The rGO/PEDOT:PSS thin films possess a RMS roughness of 1.27 nm. Previous literature reported [19] that slightly high substrate surface roughness is beneficial to perovskite crystallization process, and it causes large grain size and improved crystallinity, which is in agreement with the conclusion shown in Fig. 3.

The rGO concentration in PEDOT:PSS is regulated so as to optimize the performance of PSCs. Figure 5a shows the J–V curves of the PSC with pristine PEDOT:PSS and PSCs with rGO/PEDOT:PSS at different volume ratios. PSCs with pristine PEDOT:PSS exhibit a *Voc* of 0.85 V, a J_{SC} of 13.29 mA/cm^2, a FF of 66%, and a corresponding PCE of 8.48%. For PSCs with 0.1, 0.2, and 0.3 volume ratios of rGO/PEDOT:PSS as HTLs, the V_{OC} values are 0.90, 0.87, and 0.89 V, respectively. Correspondingly, the

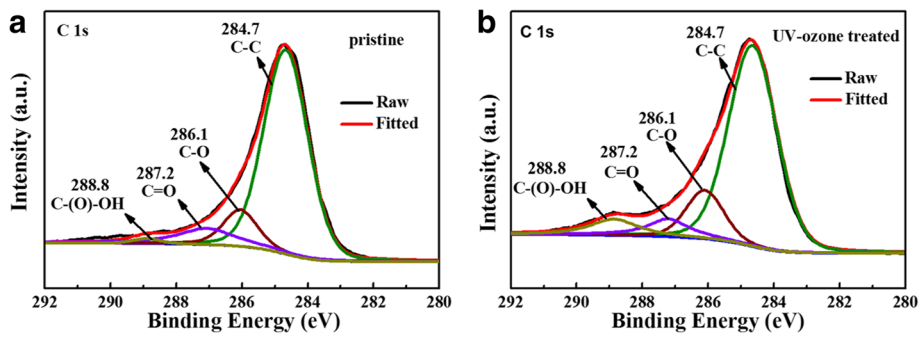

Fig. 2 XPS spectra of **a** untreated and **b** UV-ozone-treated rGO

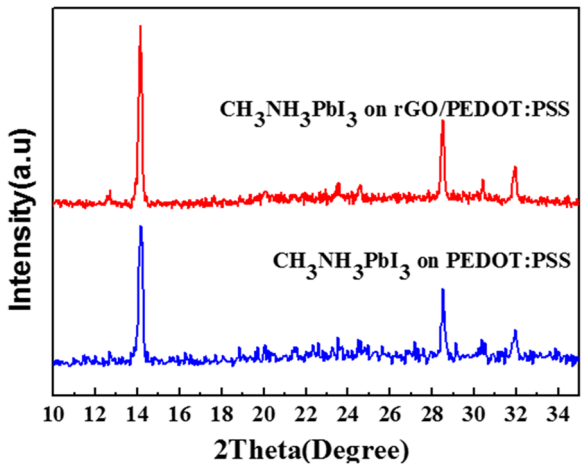

Fig. 3 XRD patterns of the perovskite films on rGO/PEDOT:PSS and PEDOT:PSS

Jsc is 15.04, 16.75, and 13.44 mA/cm^2; the FF is 66, 75, and 73%, and 68%; and the PCE is 10.16, 10.75, and 8.16%, respectively. Overall, the most remarkable device with a V_{OC} of 0.87 V, a J_{SC} of 16.75 mA/cm^2, a FF of 75%, and a PCE of 10.75% was observed in the PSCs incorporated with 0.2 *v*/*v* rGO/PEDOT:PSS as HTL. Both the V_{OC} and J_{SC} of the PSCs incorporated with 0.2 *v*/*v* rGO/PEDOT:PSS as HTL increase significantly compared with those of PSCs incorporated with pristine PEDOT:PSS as HTL. Consequently, approximately 27% enhancement was observed in the PSCs incorporated with 0.2 *v*/*v* rGO/PEDOT:PSS as HTL.

To understand the improved V_{OC} and J_{SC} for PSCs with rGO/PEDOT:PSS as HTL, Fig. 5b shows the J–V curves of PSCs with pristine PEDOT:PSS as HTL and PSCs with rGO/PEDOT:PSS (0.2 *v*/*v*) as HTL, respectively. The significantly increased value of *Jsc* is mainly due to the decreased series resistor of the device. In addition, decreased dark current also contributes to the increment of the *Jsc* of the devices according to a previous study [31–33]. To further elucidate the mechanism underlying the improvement of the device performance, the J–V curves of the devices in dark condition were also characterized. J–V measurement in the dark plays an important role in examining the diode properties of the solar cells [34]. Dark J–V measurements use electrical methods to inject carriers into the circuit rather than with photogenerated carriers to provide additional information about the cell for diagnostic purposes. The J–V curves of PSCs with pristine PEDOT:PSS as HTL and rGO/PEDOT:PSS as HTL measured in the dark are shown in Fig. 5b. The dark current value for PSCs with rGO/PEDOT:PSS as HTL is lower than that for PSCs with pristine PEDOT:PSS as HTL. This result indicated that the leakage current of the PSCs with rGO/PEDOT:PSS as HTL is suppressed. For solar cells, dark current includes reverse saturated current, thin film leakage current, and bulk leakage current. Therefore, many photogenerated charge carriers can flow through the device rather than being directly offset by dark current or shunting. Overall, the dark current is suppressed by the highly electrical conductive rGO-doped PEDOT:PSS HEL. Consequently, the V_{OC} and J_{SC} are improved, which fits with the data obtained from the dark J–V curves.

Histograms of statistical photovoltaic parameters (V_{OC}, J_{SC}, FF, and PCE) for PSCs with pristine PEDOT:PSS as HTL and rGO/PEDOT:PSS as HTL are shown in Fig. 6. Statistical data were derived from a total of 60 devices. Most of the photovoltaic parameters are in agreement with Gauss distribution despite a few experimental data, as shown in the fitting curves in Fig. 6. According to the statistical data, the V_{OC}, J_{SC}, FF,

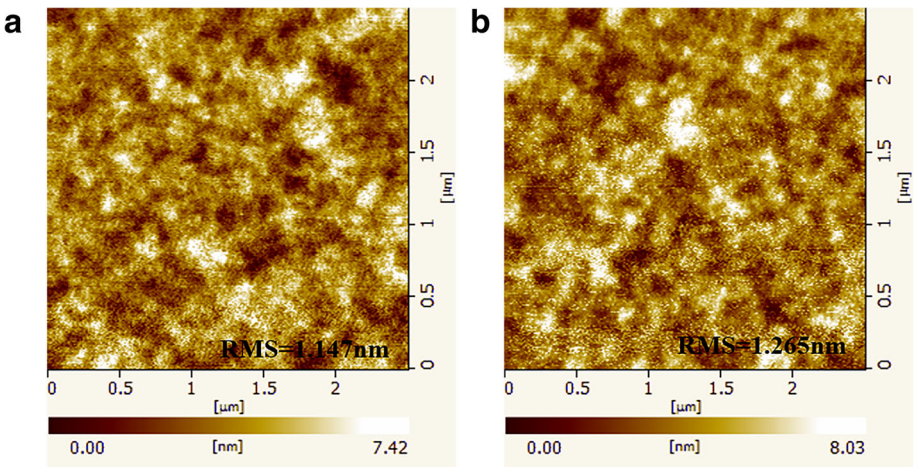

Fig. 4 AFM top-view images of **a** pristine PEDOT:PSS and **b** rGO/PEDOT:PSS thin films: all images captured an area of 2.5 × 2.5 μm^2

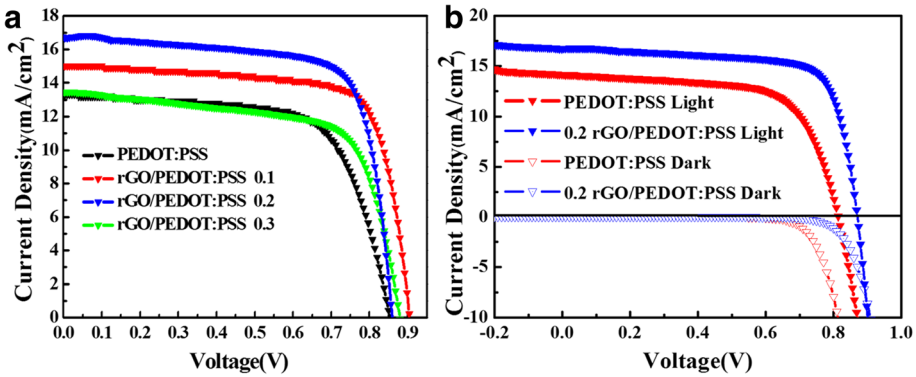

Fig. 5 **a** J–V curves of the PSC with pristine PEDOT:PSS and PSCs with rGO/PEDOT:PSS at different volume ratios. **b** J–V curves of PSCs with pristine PEDOT:PSS as HTL (red lines) and PSCs (blue lines) with rGO/PEDOT:PSS (0.2 *v/v*) as HTL measured under simulated AM1.5 sunlight of 101 mW/cm^2 irradiance (solid lines) and in the dark (dashed lines)

and PCE of PSCs with pristine PEDOT:PSS as HTL are 0.85 ± 0.01 V, 13.88 ± 0.65 mA/cm^2, 64.69 ± 1.41%, and 7.65 ± 0.48%, respectively. However, the V_{OC}, J_{SC}, FF, and PCE of PSCs with rGO/PEDOT:PSS as HTL are 0.88 ± 0.02 V, 15.25 ± 1.8 mA/cm^2, 72.37 ± 2.03%, and 9.7 ± 1.04%, respectively. In brief, the V_{OC} presents no evident change. FF and J_{SC} increase significantly, which causes a 27% enhancement of efficiency. Intrinsically, the rGO increases the *J*sc and FF of the PSCs incorporated with rGO/PEDOT:PSS as HTL. Both V_{OC} and J_{SC} of the PSCs incorporated with 0.2 *v/v* rGO/PEDOT:PSS as HTL increase significantly compared with those of PSCs incorporated with pristine PEDOT:PSS as HTL. Consequently, approximately 27% enhancement is observed in the PSCs incorporated with 0.2 *v/v* rGO/PEDOT:PSS as HTL.

Conclusions

We reported a simple and effective UV-ozone treatment method to obtain high-performance and solution-

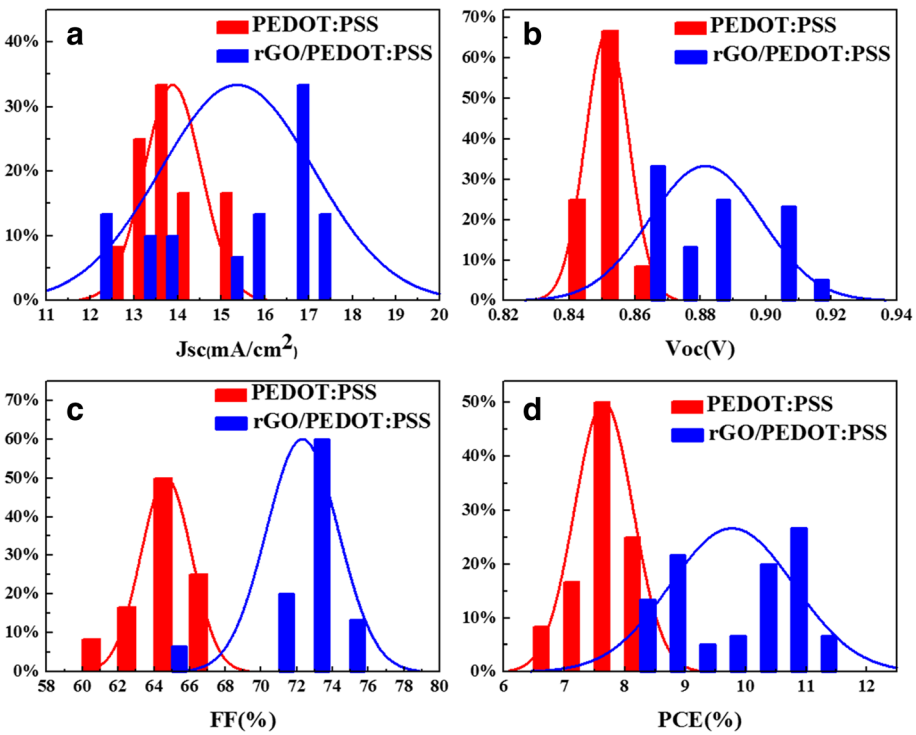

Fig. 6 Histograms of statistical photovoltaic parameters **a** V_{OC}, **b** J_{SC}, **c** FF, and **d** PCE for PSCs with pristine PEDOT:PSS as HTL and rGO/PEDOT:PSS as HTL

processable rGO. We also demonstrated the UV-ozone-treated rGO as an additive to modify the PEDOT:PSS as HTL for the fabrication of efficient PSCs. Solar cells based on treated rGO-doped PEDOT:PSS showed promising performance with a V_{OC} of 0.87 V, a J_{SC} of 16.75 mA/cm^2, a FF of 75%, and a PCE of 10.75%. Furthermore, given the excellent surface morphology and enhanced hole mobility, a 27% photoelectric conversion efficiency enhancement was observed in the PSCs incorporated with 0.2 *v*/*v* rGO/PEDOT:PSS as HTL. The distinct advantages of solution-processable rGO provide a new possibility to achieve high-efficiency solar cells and other photoelectric devices.

Acknowledgements
We acknowledge the support from the National Natural Science Foundation of China (nos. 51722204, 91421110), the National Key Basic Research Program of China (2014CB931702), and the Fundamental Research Funds for the Central University (ZYGX2016Z004).

Availability of Data and Materials
Data will not be shared.

Authors' Contributions
WSY drafted the manuscript. WSY and HXN made contribution on directing the experiments and data analysis. SHX had taken part in the acquisition and interpretation of the data. WCY formulated the idea of investigation and is the corresponding author of the work. All authors have read and approved the final manuscript.

Competing Interests
The authors declare that they have no competing interests.

Publisher's Note

Author details
[1]State Key Laboratory of Electronic Thin Films and Integrated Devices, University of Electronic Science and Technology of China, Chengdu 610054, China. [2]Chengdu NO.7 High School, Gaoxin Campus, Chengdu 610041, China. [3]Chengdu Technology University, Chengdu 611730, China.

Received: 6 November 2017 Accepted: 30 November 2017
Published online: 13 December 2017

References
1. Jeon NJ, Noh JH, Kim YC, Yang WS, Ryu S, Seok SI (2014) Solvent engineering for high-performance inorganic-organic hybrid perovskite solar cells. Nat Mater 13:897–903
2. Jeon NJ, Noh JH, Yang WS, Kim YC, Ryu S, Seo J, Seok SI (2015) Compositional engineering of perovskite materials for high-performance solar cells. Nature 517:476–480
3. Li X, Bi D, Yi C, Décoppet JD, Luo J, Zakeeruddin SM, Grätzel M (2016) A vacuum flash-assisted solution process for high-efficiency large-area perovskite solar cells. Science 353:58–62
4. Huang F, Pascoe AR, Wu WQ, Ku Z, Peng Y, Zhong J, Cheng YB (2017) Effect of the microstructure of the functional layers on the efficiency of perovskite solar cells. Adv Mater 29:1601715
5. Jeng JY, Chiang YF, Lee MH, Peng SR, Guo TF, Chen P, Wen TC (2013) $CH_3NH_3PbI_3$ perovskite/fullerene planar-heterojunction hybrid solar cells. Adv Mater 25:3727–3732
6. Nie W, Tsai H, Asadpour R, Blancon JC, Neukirch AJ, Gupta G, Wang HL (2015) High-efficiency solution-processed perovskite solar cells with millimeter-scale grains. Science 347:522–525
7. Chen W, Wu Y, Yue Y, Liu J, Zhang W, Yang X, Han L (2015) Efficient and stable large-area perovskite solar cells with inorganic charge extraction layers. Science 350:944–948
8. Chiang CH, Wu CG (2016) Bulk heterojunction perovskite–PCBM solar cells with high fill factor. Nat Photon 10:196–200
9. Liu T, Chen K, Hu Q, Zhu R, Gong Q (2016) Inverted perovskite solar cells: progresses and perspectives. Adv Energy Mater 6:1600457
10. Castro E, Zavala G, Seetharaman S, D'Souzab F, Echegoyen L (2017) Impact of fullerene derivative isomeric purity on the performance of inverted planar perovskite solar cells. J Mater Chem A 5(36):19485–19490
11. Chiang CH, Nazeeruddin MK, Grätzel M, Wu CG (2017) The synergistic effect of H_2O and DMF towards stable and 20% efficiency inverted perovskite solar cells. Energy Environ Sci 10(3):808–817
12. Malinkiewicz O, Yella A, Lee YH, Espallargas GM, Graetzel M, Nazeeruddin MK, Bolink HJ (2014) Perovskite solar cells employing organic charge-transport layers. Nat Photon 8:128–132
13. Zhu Z, Bai Y, Zhang T, Liu Z, Long X, Wei Z, Yang S (2014) High-performance hole-extraction layer of sol-gel-processed NiO nanocrystals for inverted planar perovskite solar cells. Angew Chem 53:12571–12575
14. Capasso A, Matteocci F, Najafi L, Prato M, Buha J, Cinà L, Bonaccorso F (2016) Few-layer MoS_2 flakes as active buffer layer for stable perovskite solar cells. Adv Energy Mater 6:1600920
15. Zhou P, Fang Z, Zhou W, Qiao Q, Wang M, Chen T, Yang S (2017) Non-conjugated polymer poly (vinylpyrrolidone) as an efficient interlayer promoting electron transport for perovskite solar cells. ACS Appl Mater Interfaces 9:32957–32964
16. Sun C, Wu Z, Yip HL, Zhang H, Jiang XF, Xue Q, Huang F (2016) Amino-functionalized conjugated polymer as an efficient electron transport layer for high-performance planar-heterojunction perovskite solar cells. Adv Energy Mater 6:1501534
17. Kim HB, Choi H, Jeong J, Kim S, Walker B, Song S, Kim JY (2014) Mixed solvents for the optimization of morphology in solution-processed, inverted-type perovskite/fullerene hybrid solar cells. Nano 6:6679–6683
18. Eperon GE, Burlakov VM, Docampo P, Goriely A, Snaith HJ (2014) Morphological control for high performance, solution-processed planar heterojunction perovskite solar cells. Adv Funct Mater 24:151–157
19. Yu JC, Kim DB, Baek G, Lee BR, Jung ED, Lee S, Song MH (2015) High-performance planar perovskite optoelectronic devices: a morphological and interfacial control by polar solvent treatment. Adv Mater 27:3492–3500
20. Chen W, Xu L, Feng X, Jie J, He Z (2017) Metal acetylacetonate series in interface engineering for full low-temperature-processed, high-performance, and stable planar perovskite solar cells with conversion efficiency over 16% on 1 cm^2 scale. Adv Mater 29:1603923
21. Yu M, Huang X, Wang S, Chen B, Zhang Y, Chen B, Xiong J (2017) Enhancing performance of inverted planar perovskite solar cells by argon plasma post-treatment on PEDOT: PSS. RSC Adv 7:17398–17402
22. Correa-Baena JP, Abate A, Saliba M, Tress W, Jacobsson TJ, Grätzel M, Hagfeldt A (2017) The rapid evolution of highly efficient perovskite solar cells. Energy Environ Sci 10:710–727
23. Huang X, Guo H, Yang J, Wang K, Niu X, Liu X (2016) Moderately reduced graphene oxide/PEDOT: PSS as hole transport layer to fabricate efficient perovskite hybrid solar cells. Org Electron 39:288–295
24. Yin Z, Zhu J, He Q, Cao X, Tan C, Chen H, Zhang H (2014) Graphene-based materials for solar cell applications. Adv Energy Mater 4:1300574
25. Sun H, Lei T, Tian W, Cao F, Xiong J, Li L (2017) Self-powered, flexible and solution-processable perovskite photodetector based on low-cost carbon cloth. Small 13:1701042
26. Yeo JS, Kang R, Lee S, Jeon YJ, Myoung N, Lee CL, Na SI (2015) Highly efficient and stable planar perovskite solar cells with reduced graphene oxide nanosheets as electrode interlayer. Nano Energy 12:96–104
27. Jokar E, Huang ZY, Narra S, Wang CY, Kattoor V, Chung CC, Diau EWG (2017) Anomalous charge-extraction behavior for graphene-oxide (GO) and reduced graphene-oxide (rGO) films as efficient p-contact layers for high-performance perovskite solar cells. Adv Energy Mater. https://doi.org/10.1002/aenm.201701640
28. Zhu Z, Ma J, Wang Z, Mu C, Fan Z, Du L, Yang S (2014) Efficiency enhancement of perovskite solar cells through fast electron extraction: the role of graphene quantum dots. J Am Chem Soc 136:3760–3763
29. He JR, Chen YF, Li PJ, Wang ZG, Qi F, Liu JB (2014) Synthesis and electrochemical properties of graphene-modified $LiCo_{1/3}Ni_{1/3}Mn_{1/3}O_2$ cathodes for lithium ion batteries. RSC Adv 4:2568–2572

30. Xiao M, Huang F, Huang W, Dkhissi Y, Zhu Y, Etheridge J, Spiccia L (2014) A fast deposition-crystallization procedure for highly efficient lead iodide perovskite thin-film solar cells. Angew Chem 126:10056–10061
31. Luo Q, Zhang Y, Liu C, Li J, Wang N, Lin H (2015) Iodide-reduced graphene oxide with dopant-free spiro-OMeTAD for ambient stable and high-efficiency perovskite solar cells. J Mater Chem A 3:15996–16004
32. Wang Y, Wu J, Zhang P, Liu D, Zhang T, Ji L, Gu X, Chen ZD, Li S (2017) Stitching triple cation perovskite by a mixed anti-solvent process for high performance perovskite solar cells. Nano Energy 39:616–625
33. Zhang P, Wu J, Wang Y, Sarvari H, Liu D, Chen ZD, Li S (2017) Enhanced efficiency and environmental stability of planar perovskite solar cells by suppressing photocatalytic decomposition. J Mater Chem A 5(33):17368–17378
34. Peshek TJ, Zhang L, Singh RK, Tang Z, Vahidi M, B. To, Schilfgaarde M (2013) Criteria for improving the properties of $ZnGeAs_2$ solar cells. Prog Photovoltaics 21:906–917